Letters

6.78-MHz Wireless Power Transfer With Self-Resonant Coils at 95% DC–DC Efficiency

Lei Gu, *Member, IEEE*, Grayson Zulauf, *Student Member, IEEE*, Aaron Stein, Phyo Aung Kyaw, Tuofei Chen, *Student Member, IEEE*, and Juan Manuel Rivas Davila, *Senior Member, IEEE*

***Abstract*—Megahertz-frequency inductive wireless power transfer holds the promise of compact and efficient wireless power transfer. Unfortunately, due to high-frequency losses in wide-bandgap semiconductors and low-Q high-frequency coil designs, these systems are universally less efficient, on a dc–dc basis, than wireless power systems operating at conventional frequency regimes. This letter describes the design considerations for inductive wireless power transfer systems operating at 6.78 MHz. With a novel high-frequency resonant amplifier topology, a high-Q self-resonant coil structure, and a better understanding of C_{oss} losses in wide-bandgap power semiconductors, we demonstrate 6.78- MHz wireless power transfer systems that achieve 95% dc–dc efficiency at power levels up to and beyond 1 kW.**

***Index Terms*—Coupling circuits, electromagnetic coupling, inductive charging, power amplifiers, tuning, wireless power transmission, zero voltage switching.**

I. Introduction

INDUCTIVE wireless power transfer (WPT) has the potential to improve the convenience, cost, and utilization of battery-powered systems, including electric vehicles, medical implants, and robotics for warehouse automation.

Wireless chargers typically operate with a switching frequency of 20–200 kHz [1], [2], resulting in electromagnetic coils that dominate the cost, weight, size, and losses of the wireless charging system [3]. Increasing the frequency has the potential to improve coil power density, efficiency, and cost through the increase in coil quality factor expected with higher frequency [4], and beyond 200 kHz, the international, scientific, and medical band of 6.78 MHz is an attractive frequency of operation from a regulatory and standardization perspective [5].

Winding loss is a critical, and often dominant, component of the power losses in the WPT coils. One promising avenue to decrease winding loss is by increasing the switching frequency (f_{sw}), where the quality factor (Q) is expected to increase with f_{sw} [6]. More tangibly, if the conductors are fully utilized, increasing the switching frequency from 200 kHz to 6.78 MHz would allow 33$\times$ less copper to be used to achieve the same performance—or, alternatively, the same amount of fully utilized copper could increase Q by the identical 33$\times$ factor (or winding loss would no longer dominate the coil losses). At megahertz (MHz) frequencies, further, the benefit of using litz wire is limited [7], and the cost of the coils can be reduced by replacing litz wire with solid wire or thin foil layers. With emerging wide-bandgap (WBG) power semiconductors, such as GaN and SiC, that have excellent $R_{\text{DS,on}} * Q_{\text{g}}$ figures-of-merit relative to Si devices [8], the high-frequency inverter and rectifier may also operate with high efficiency, even at MHz frequencies. With the coils improved at high frequency and new power electronics devices and topologies enabling fast switching operation, the promise of high efficiency and compact dc–dc MHz WPT systems can be realized.

Despite this potential, the high-frequency promise has not been realized in WPT, as shown in the survey of existing WPT dc–dc converters of Fig. 1. Only a single system with f_{sw} above 1 MHz has achieved a dc–dc efficiency above 90% [12], nearly 2$\times$ higher losses than the highly efficient performance in the 20–200 kHz switching range (95%) [10], [11]. These low reported efficiencies are due to two primary drivers: high-frequency design challenges in the inverter and rectifier, where power semiconductor losses—even with soft switching—are much higher than expected [23], [24], and low-Q coils and resonant tanks at MHz frequencies [22].

In this letter, we take on all of these challenges—combining new topologies [25]–[28], SOA coils [29], and a deep understanding of high-frequency losses in power semiconductors [23], [30]—to showcase two benchmark setting 6.78- MHz wireless power systems with a best-in-class dc–dc efficiency of 95% at maximum output power levels of 300 and 1 kW. These new benchmarks, which are 2$\times$ lower losses than the best existing multi-MHz WPT systems, indicate that with careful design of

Manuscript received June 12, 2020; revised July 13, 2020; accepted July 28, 2020. Date of publication August 5, 2020; date of current version October 30, 2020. This work was supported in part by the Center for Automotive Research at Stanford (CARS) Postdoctoral Fellowship, in part by a Precourt Institute for Energy Seed Grant, in part by the National Science Foundation, and in part by the Stanford Graduate Fellowship Program. *(Corresponding author: Lei Gu.)*

Lei Gu, Grayson Zulauf, Tuofei Chen, and Juan Manuel Rivas Davila are with the Department of Electrical Engineering, Stanford University, Stanford, CA 94305 USA (e-mail: leigu@stanford.edu; gzulauf@stanford.edu; tfchen@stanford.edu; jmrivas@stanford.edu).

Aaron Stein and Phyo Aung Kyaw are with the Resonant Link, LLC, Shelburne, VT 05482 USA (e-mail: astein@resonant-link.com; albert.phyoaungkyaw@gmail.com).

Color versions of one or more of the figures in this article are available online at https://ieeexplore.ieee.org.

Digital Object Identifier 10.1109/TPEL.2020.3014042

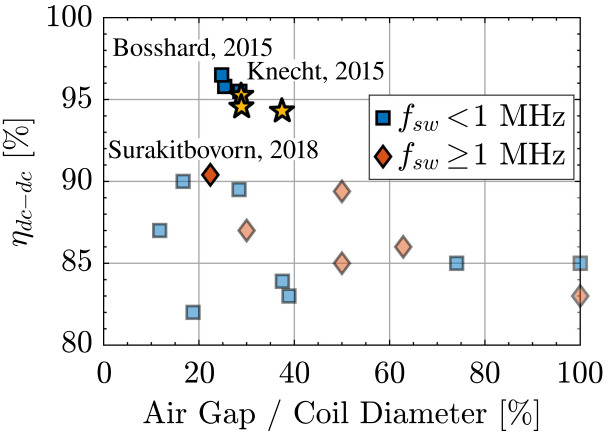

Fig. 1. DC–DC efficiency for state-of-the-art (SOA) WPT. Existing systems with switching frequencies below 1 MHz achieve dc–dc efficiencies over 95%, but prior multi-MHz designs had only reached 90%, a 2× increase in losses for a similar coupling coefficient. This work (⋆) realizes highly efficient (> 95%) and ultracompact dc–dc WPT converters at 6.78 MHz and over 1- kW output power. Directly cited work is [9]–[12], and backgrounded SOA is [13]–[22] and two commercial systems, WiTricity ICS115 and D-Broad Core.

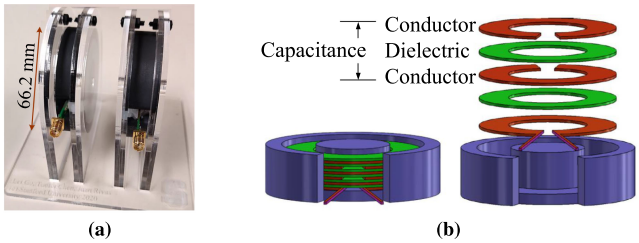

Fig. 2. Implemented coils in this letter. (a) Coils, with a diameter of 6.6 cm. (b) MSRS internal architecture, with an integrated capacitance and thin foil layers [29].

both power electronics and electromagnetics, the promise of increased frequency can be realized in ultracompact and highly efficient wireless power links to power the electric, automated future of logistics (robots, drones) and transportation (scooters, electric vehicles).

II. Parallel-Compensated Coil Considerations

Recently, an integrated WPT coil design—where the compensation capacitance is embedded into the winding of the coil—was published in [29], which achieves Q that is 6× higher than the best conventional designs (with similar dimensions) at 6.78 MHz. The coil architecture, which is shown in Fig. 2 and termed as the multilayer self-resonant structure (MSRS), utilizes the compensation capacitance to force equal current sharing among multiple thin foil layers, mitigating both the skin and proximity effects that typically drive winding losses at multi-MHz frequencies. Although this coil achieves a very high quality factor, the structure is inherently parallel-compensated. There are limited publications that discuss a parallel–parallel (PP) compensated design (versus the more standard series–series or series–parallel compensation strategies [31]), and this section focuses on the design of the WPT system around this parallel-compensated architecture.

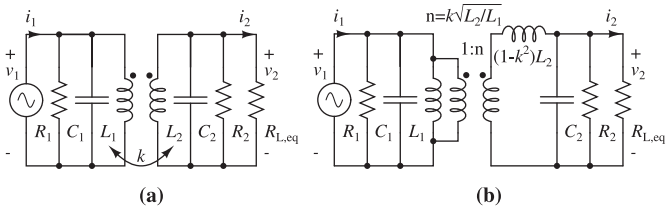

Fig. 3. Coupled parallel-compensated coils circuit model. (a) Coupled circuit model. (b) Cantilever model.

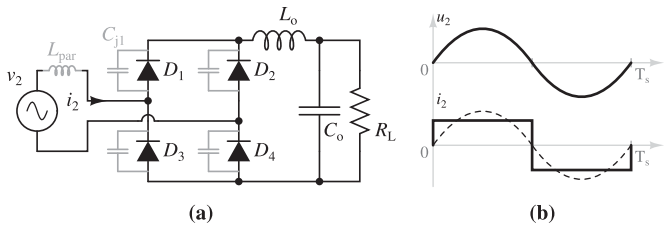

Fig. 4. Current-mode rectifier. (a) Circuit. (b) Ideal waveform.

Parallel-compensated coils can be modeled, as shown in Fig. 3. The cantilever model of Fig. 3(b) is simple to measure and understand [32], whereas the coupled-coil model in Fig. 3(a) gives more insight to the circuit operation. The lumped resistances R_1 and R_2 model the total losses of the respective resonant tanks. Because the compensation capacitances C_1 and C_2 are in parallel with the resonator terminals, the voltage across the two tanks cannot change instantaneously, preventing the use of voltage-mode inverter and rectifier circuits.

A current-mode rectifier is suitable to rectify the output of a parallel-compensated coil on the secondary side, as shown in Fig. 4. Here, the current-mode rectifier has a choke inductor output filter L_o,[1] and the dc output current can be approximated as constant. In the current-mode rectifier, the ac voltage has low distortion and is close to a sine wave and the ac current is a square wave.

Ideally, a current-mode rectifier can be modeled as an equivalent resistance with a value of $R_{\mathrm{L,eq}} = \frac{\pi^2}{8} R_{\mathrm{L}}$ [32], but the junction capacitance of the diodes makes the effective input impedance slightly capacitive. This part of the capacitive impedance must be considered and calculated, and when known, can be incorporated into the compensation capacitance C_2. This capacitive impedance, however, depends on the large-signal behavior of the rectifier and does not simply equal the sum of the small signal junction capacitance of the diodes.

To achieve the maximum wireless link efficiency of Waffenschmidt and Staring [33], the compensation capacitance must correctly resonate with the coil inductance. For PP compensation, the relationship between the inductances and the capacitances of the coils is

$$C_1 = \frac{1}{\omega_0^2 L_1 (1-k^2)} \quad C_2 = \frac{1}{\omega_0^2 L_2 (1-k^2)} \tag{1}$$

where the capacitance is selected to cancel the leakage inductance on each side. Practically, these can be quickly tuned by

[1] A voltage-mode rectifier only has a capacitive output filter and works with series-compensated coils.

ensuring that L and C resonate at the switching frequency with the opposite coil terminals shorted.

P_1, P_2, and P_{loss} are the input, output power, and the total losses of the wireless link, respectively. Q_1 and Q_2 are the quality factors of the coils

$$Q_1 = \frac{R_1}{\omega_0 L_1},\ Q_2 = \frac{R_2}{\omega_0 L_2}. \tag{2}$$

We define the load matching factor γ as the ratio between the secondary-side coil impedance and the equivalent ac load resistance

$$\gamma = \frac{\omega_0 L_2}{R_{\text{L,eq}}}. \tag{3}$$

For a design using (1), we can calculate the total loss factor $\lambda = P_{\text{loss}}/P_2$ as

$$\lambda = \frac{1}{\gamma Q_2} + \frac{\left(1-k^2\right)^2}{k^2}\frac{1}{\gamma Q_1}\left(\gamma + \frac{1}{Q_2}\right)^2. \tag{4}$$

Furthermore, the maximum WPT link efficiency is achieved when λ is minimum, so the load must be optimized relative to the impedance of the receive coil as

$$\gamma_{\text{opt}} = \frac{1}{Q_2}\sqrt{1+\left(\frac{k}{1-k^2}\right)^2 Q_1 Q_2}. \tag{5}$$

With high-Q coils, $kQ_1, kQ_2 >> 1$

$$\gamma_{\text{opt}} \approx \sqrt{\frac{Q_1}{Q_2}}\frac{k}{1-k^2}. \tag{6}$$

If symmetric coils are used, the quality factors will be similar, $Q_1 \approx Q_2$, the optimal load matching factor becomes

$$\gamma_{\text{opt}} \approx \frac{k}{1-k^2}. \tag{7}$$

In the following sections, we showcase this understanding of driving and rectifying these high-Q, parallel-compensated, self-resonant coils with two candidate inverter topologies showcasing high efficiency (>95%), 6.78-MHz WPT with both legacy Si MOSFETs and next-generation GaN power semiconductors.

III. 300-W System Using a Novel Φ_2 Amplifier

As mentioned earlier, the voltage across the primary coil cannot change instantaneously due to the parallel compensation. The resonant inverter needs to behave more like a power amplifier, where the output voltage has low harmonic distortion, and a conventional half-bridge circuit cannot drive a parallel resonator directly (unlike for series-compensated coils). In the following sections, we introduce two high-efficiency amplifier topologies that are suitable for driving parallel-compensated primary coils.

Gu *et al.* [25] and Gu [34] introduced a novel push–pull Φ_2 amplifier topology that uses a T network for impedance tuning, which is termed a PPT Φ_2 amplifier. The amplifier achieves both low switch voltage stress and simplicity of gate driving. Fig. 5 shows the schematic of the PPT Φ_2 amplifier driving the parallel-compensated coils and a current-mode rectifier. With a series-stacked structure, S_1 and S_2 have a peak voltage stress of $1.05V_{\text{i}}$,

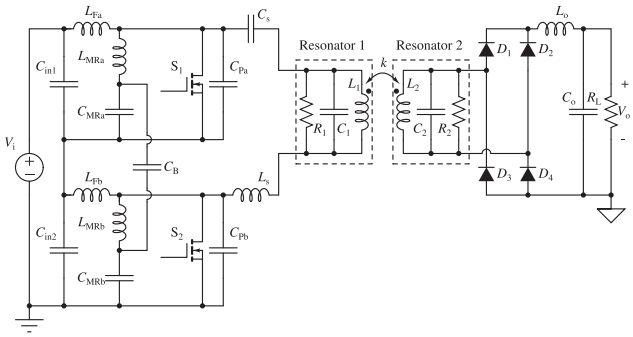

Fig. 5. Schematic of the PPT Φ_2 wireless dc–dc converter.

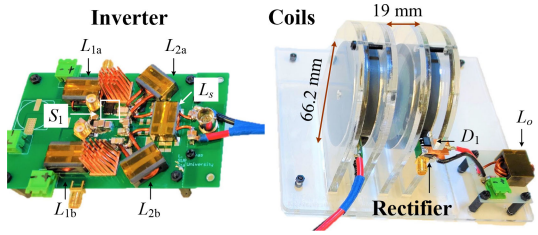

Fig. 6. Photograph of the PPT Φ_2 wireless dc–dc converter. Coil diameter is 66.2 mm and the separation between the closest part of the coils is 19 mm. Implemented inverter dimensions are 7 cm × 7 cm × 1 cm. Diodes are integrated on coil output terminal for low parasitic inductance.

TABLE I
Bill of Materials, PPT Φ_2 WPT DC–DC Converter

Device Symbols	Component Description
$S_{1,2}$	Infineon BSC160N15NS5 150 V Si MOSFET
$D_{1\text{-}4}$	STMicro STPSC406B-TR 650 V SiC Schottky
L_{Fa}, L_{Fb}	1.46 µH, Fair-rite 67 EEQ20/9
L_{MRa}, L_{MRb}	297 nH, Fair-rite 67 EEQ20/9
C_{MRa}, C_{MRb}	451 pF , C0G ceramic, 500 V
C_{Pa}, C_{Pb}	S_1 C_{oss} + 630 pF, C0G ceramic, 500 V
L_s	1.1 µH, Fair-rite 67 EEQ20/13
C_s	550 pF, C0G ceramic, 200 V
L_{o}	7 µH, Ferroxcube E22/6/16-4F1

much lower than the stress of a conventional Class-E [35] (3.6 V_{i}) and its variants like the Class-EF$_2$ [36] (2.1V_{i}). The voltage on C_{in1} and C_{in2} is half of the input $0.5V_{\text{i}}$ and is automatically balanced because of the push–pull operation between S_1 and S_2. The source of S_1 is referred to a constant dc potential ($0.5V_{\text{i}}$) that simplifies the gate drive implementation relative to a half-bridge circuit. The PPT Φ_2 can maintain zero-voltage-switching (ZVS) operation across a wide resistive load range, which is advantageous for driving the parallel-compensated WPT coils.

At the resonant frequency, the input impedance to the coils stays resistive across variable output loads. Fig. 6 shows the prototype PPT Φ_2 wireless dc–dc converter that matches the schematic in Fig. 5. Table I lists the key components for the 300-W Φ_2 wireless dc–dc converter, and Table II lists the parameters of the WPT coils. The prototype uses 150-V Si MOSFETs and 650-V SiC Schottky didoes. Using low-voltage Si trench MOSFETs eliminates the additional C_{oss} and dynamic on-resistance losses in high-voltage GaN FETs at MHz frequencies [23], [30].

TABLE II
MSRS COIL PARAMETERS

L_1 [H]	C_1 [F]	R_1 [Ω]	Q_1	L_2 [H]	C_2 [F]	R_2 [Ω]	Q_2
166.5n	3.32n	5.02k	708	159.3n	3.36n	4.84k	713

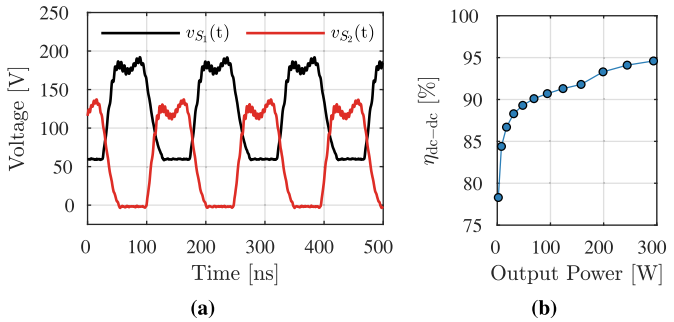

Fig. 7. PPT Φ_2 wireless prototype experimental (a) drain voltage waveform and (b) efficiency performance. Gate driving losses excluded. Power varied by adjust input voltage.

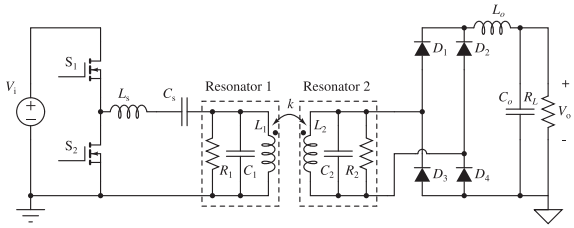

Fig. 8. Schematic of the Class-D wireless dc–dc converter.

Among the available Si and SiC diodes we tested [24], we selected the SiC Schottky diode with the least total conduction and C_{oss} losses for this voltage and power level. The equivalent large signal capacitance of the rectifier is roughly 175 pF at 120 V_{out}. At a separation of 19 mm, the coupling between the coils is $k = 0.15$, a low coupling compared to many of the SOA shown in Fig. 1. Fig. 7 shows the measured drain node voltage waveform and efficiency performance of the prototype, with the converter continuously delivering 300 W from 120 V_{in} to 120 V_{out} with a dc–dc efficiency of 94.6% at 6.78 MHz.

With this proof-of-concept of ultrahigh-efficiency 6.78-MHz wireless power even with legacy Si MOSFETs, we move to extend the power to the kilowatt (kW) scale with an alternate inverter topology and modern WBG power semiconductors.

IV. 1-kW System Using a Class-D Amplifier

Another MHz-frequency amplifier suitable for driving parallel-compensated coils is the Class-D amplifier with a high-Z series tank. Fig. 8 shows the schematic of the Class-D amplifier to drive the parallel coils, and a current-mode rectifier for the high-frequency rectification. Because of the shunt capacitance, the series filter L_s–C_s is necessary to remove the high-frequency harmonics, help achieve ZVS operation, and make the drive appear more "current-mode-like" to the shunt capacitances of the parallel-compensated coils.

Fig. 9 shows the photograph of the prototype converter, with

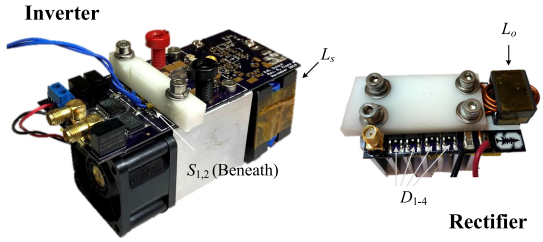

Fig. 9. Photograph of the 1-kW Class-D inverter and current-mode rectifier. Implemented inverter dimensions are 11.3 cm × 5.8 cm × 6 cm. Full-bridge current-mode diode rectifier (SiC Schottky diodes under clamping plate) dimensions are 6.7 cm × 3.7 cm × 3.7 cm.

TABLE III
BILL OF MATERIALS, CLASS-D WPT DC–DC CONVERTER

Device Symbols	Component Description
$S_{1,2}$	GaN Systems GS66508P 650 V GaN FET
$D_{1\text{-}4}$	STMicro STPSC406B-TR x2 650 V SiC Schottky
L_s	950 nH, Ferroxcube E58/11/38-4F1
C_s	8 nF, C0G ceramic, 1500 V
L_o	7 µH, Ferroxcube E22/6/16-4F1

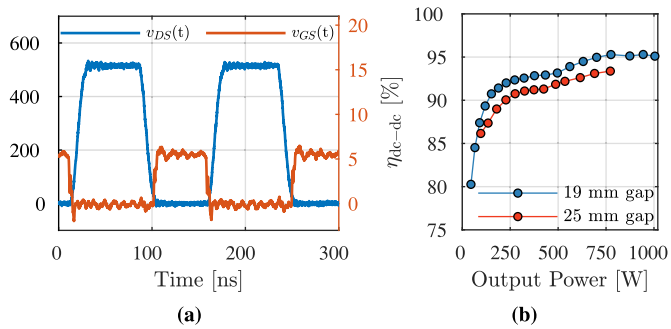

Fig. 10. Class D wireless prototype experimental (a) drain and gate voltage waveform at 525 V_{in} and (b) efficiency performance across output power. Gate driving losses excluded. Power is varied by adjusting the input voltage.

same coils as those in Fig. 6 and Table II (with a slight adjustment to the compensation capacitance) used here. The Class-D implementation uses 650-V GaN FETs and 650-V SiC Schottky diodes (two in parallel for each diode), with the specific GaN and SiC devices selected to minimize the total device losses, including the large C_{oss} losses at this frequency and voltage level [23], [24] and the dynamic on-resistance losses [30]. The inclusion of C_{oss} losses and dynamic R_{on} effect pushes the preferred operating point to have lower current and lower *dV/dt* to reduce both conduction and C_{oss} losses.

Fig. 10(a) shows the drain node at 525 V_{in}, where we observe ZVS, and Fig. 10(b) shows the measured dc–dc efficiency of the prototype as the power level is increased by increasing the input voltage. The prototype delivers 1-kW continuous power from 525 V_{in} to 225 V_{out} with a dc–dc efficiency of 95.1% at 6.78 MHz, with a peak efficiency of 95.3% at 943-W continuous output power. The equivalent large signal input capacitance of the rectifier is roughly 330 pF at 223 V_{out}. Again, multi-MHz WPT is shown to achieve dc–dc efficiencies comparable to

is increased to the kW-scale with an eye toward charging the drones, scooters, robots, and electric vehicles of the logistics and transportation futures.

V. Conclusion

High-frequency WPT can be more cost-effective and compact than conventional litz-based, kHz-frequency WPT systems, but the efficiency of existing MHz-frequency systems has been limited by both poorly understood power semiconductor losses and low-Q coil designs, and the losses at MHz frequencies have been about $2\times$ higher than comparable systems in the kHz regime. In this letter, we combine a novel high-frequency resonant amplifier topology, high-Q self-resonant coils, and a better understanding of high-frequency losses (C_{oss} losses and dynamic on-resistance) in WBG devices to showcase kW-scale 6.78-MHz WPT systems with dc–dc efficiencies above 95% and coil power densities as high as 30 W/cm^2. These benchmark-setting prototypes highlight the promise of high-frequency, high-power WPT.

References

[1] "Wireless power consortium, Qi certified products," Accessed: Oct. 1, 2019. [Online]. Available: https://www.wirelesspowerconsortium.com/knowledge-base/testing-and-cert% ification/qi-certified-products.html

[2] *Wireless Power Transfer for Light-Duty Plug-In/Electric Vehicles and Alignment Methodology*, SAE International, Warrendale, PA, USA, J2954_201711, Nov. 2017.

[3] A. Shekhar, V. Prasanth, P. Bauer, and M. Bolech, "Economic viability study of an on-road wireless charging system with a generic driving range estimation method," *Energies*, vol. 9, no. 2, 2016, Art. no. 76.

[4] A. J. Hanson, J. A. Belk, S. Lim, C. R. Sullivan, and D. J. Perreault, "Measurements and performance factor comparisons of magnetic materials at high frequency," *IEEE Trans. Power Electron.*, vol. 31, no. 11, pp. 7909–7925, Nov. 2016.

[5] International Commission on Non-Ionizing Radiation Protection and others, "Guidelines for limiting exposure to electromagnetic fields (100 kHz to 300 GHz)," *Health Phys.*, vol. 118, no. 5, pp. 483–524, 2020.

[6] C. R. Sullivan, B. A. Reese, A. L. F. Stein, and P. A. Kyaw, "On size and magnetics: Why small efficient power inductors are rare," in *Proc. IEEE Int. Symp. 3D Power Electron. Integr. Manuf.*, 2016, pp. 1–23.

[7] C. R. Sullivan, "High-frequency magnetics design: Overview and winding loss," 2016. [Online]. Available: https://www.psma.com/sites/default/files/uploads/tech-forums-magnetics/%presentations/high-frequency-magnetics-design-overview-and-winding-loss.pdf

[8] H. Okumura, "A roadmap for future wide bandgap semiconductor power electronics," *MRS Bull.*, vol. 40, no. 5, pp. 439–444, 2015.

[9] R. Bosshard and J. W. Kolar, "Multi-objective optimization of 50 kW/85 kHz IPT system for public transport," *IEEE J. Emerg. Sel. Topics Power Electron.*, vol. 4, no. 4, pp. 1370–1382, Dec. 2016.

[10] R. Bosshard, J. W. Kolar, J. Mühlethaler, I. Stevanović, B. Wunsch, and F. Canales, "Modeling and $\eta-\alpha-$pareto optimization of inductive power transfer coils for electric vehicles," *IEEE J. Emerg. Sel. Topics Power Electron.*, vol. 3, no. 1, pp. 50–64, Mar. 2015.

[11] O. Knecht, R. Bosshard, and J. W. Kolar, "High-efficiency transcutaneous energy transfer for implantable mechanical heart support systems," *IEEE Trans. Power Electron.*, vol. 30, no. 11, pp. 6221–6236, Nov. 2015.

[12] K. Surakitbovorn and J. Rivas-Davilla, "Design of a GaN-based wireless power transfer system at 13.56 MHz to replace conventional wired connection in a vehicle," in *Proc. IEEE Int. Power Electron. Conf.*, 2018, pp. 3848–3854.

[13] J. M. Arteaga, S. Aldhaher, G. Kkelis, C. Kwan, D. C. Yates, and P. D. Mitcheson, "Dynamic capabilities of multi-MHz inductive power transfer systems demonstrated with batteryless drones," *IEEE Trans. Power Electron.*, vol. 34, no. 6, pp. 5093–5104, Jun. 2019.

[14] J. M. Arteaga *et al.*, "Multi-MHz IPT systems for variable coupling," *IEEE Trans. Power Electron.*, vol. 33, no. 9, pp. 7744–7758, Sep. 2018.

[15] Z. Huang, S. Wong, and C. K. Tse, "Control design for optimizing efficiency in inductive power transfer systems," *IEEE Trans. Power Electron.*, vol. 33, no. 5, pp. 4523–4534, May 2018.

[16] M. Liu, M. Fu, and C. Ma, "Low-harmonic-contents and high-efficiency class E full-wave current-driven rectifier for megahertz wireless power transfer systems," *IEEE Trans. Power Electron.*, vol. 32, no. 2, pp. 1198–1209, Feb. 2017.

[17] H. Li, K. Wang, J. Fang, and Y. Tang, "Pulse density modulated ZVS full-bridge converters for wireless power transfer systems," *IEEE Trans. Power Electron.*, vol. 34, no. 1, pp. 369–377, Jan. 2019.

[18] H. Li, J. Li, K. Wang, W. Chen, and X. Yang, "A maximum efficiency point tracking control scheme for wireless power transfer systems using magnetic resonant coupling," *IEEE Trans. Power Electron.*, vol. 30, no. 7, pp. 3998–4008, Jul. 2015.

[19] H. Li, J. Fang, S. Chen, K. Wang, and Y. Tang, "Pulse density modulation for maximum efficiency point tracking of wireless power transfer systems," *IEEE Trans. Power Electron.*, vol. 33, no. 6, pp. 5492–5501, Jun. 2018.

[20] C. Cheng *et al.*, "Load-independent wireless power transfer system for multiple loads over a long distance," *IEEE Trans. Power Electron.*, vol. 34, no. 9, pp. 9279–9288, Sep. 2019.

[21] W. Zhang, S. Wong, C. K. Tse, and Q. Chen, "Design for efficiency optimization and voltage controllability of series–series compensated inductive power transfer systems," *IEEE Trans. Power Electron.*, vol. 29, no. 1, pp. 191–200, Jan. 2014.

[22] G. Zulauf and J. M. Rivas-Davila, "Single-turn air-core coils for high-frequency inductive wireless power transfer," *IEEE Trans. Power Electron.*, vol. 35, no. 3, pp. 2917–2932, Mar. 2020.

[23] G. Zulauf, S. Park, W. Liang, K. N. Surakitbovorn, and J. Rivas-Davila, "C_{oss} losses in 600 V GaN power semiconductors in soft-switched, high- and very-high-frequency power converters," *IEEE Trans. Power Electron.*, vol. 33, no. 12, pp. 10748–10763, Dec. 2018.

[24] Z. Tong, G. Zulauf, J. Xu, J. D. Plummer, and J. Rivas-Davila, "Output capacitance loss characterization of silicon carbide Schottky diodes," *IEEE J. Emerg. Sel. Topics Power Electron.*, vol. 7, no. 2, pp. 865–878, Jun. 2019.

[25] L. Gu, G. Zulauf, Z. Zhang, S. Chakraborty, and J. Rivas-Davila, "Push–pull class Φ_2 RF power amplifier," *IEEE Trans. Power Electron.*, vol. 35, no. 10, pp. 10515–10531, Oct. 2020.

[26] L. Gu, K. Surakitbovorn, G. Zulauf, S. Chakraborty, and J. Rivas-Davila, "High-frequency bidirectional resonant converter for high conversion ratio and variable load operation," *IEEE J. Emerg. Sel. Topics Power Electron.*, vol. 8, no. 3, pp. 1983–1993, Sep. 2020.

[27] L. Gu, W. Liang, L. C. Raymond, and J. Rivas-Davila, "27.12 MHz GaN bi−directional resonant power converter," in *Proc. IEEE 16th Workshop Control Model. Power Electron.*, 2015, pp. 1–7.

[28] L. Gu, W. Liang, and J. R. Davila, "Design of very-high-frequency synchronous resonant DC-DC converter for variable load operation," in *Proc. IEEE Energy Convers. Congr. Expo.*, Oct. 2017, pp. 3447–3454.

[29] A. L. F. Stein, P. A. Kyaw, and C. R. Sullivan, "Wireless power transfer utilizing a high-Q self-resonant structure," *IEEE Trans. Power Electron.*, vol. 34, no. 7, pp. 6722–6735, Jul. 2019.

[30] G. Zulauf, M. Guacci, and J. W. Kolar, "Dynamic on-resistance in GaN-on-Si HEMTs: Origins, dependencies, and future characterization frameworks," *IEEE Trans. Power Electron.*, vol. 35, no. 6, pp. 5581–5588, Jun. 2020.

[31] O. Knecht and J. W. Kolar, "Comparative evaluation of IPT resonant circuit topologies for wireless power supplies of implantable mechanical circulatory support systems," in *Proc. IEEE Appl. Power Electron. Conf. Expo.*, 2017, pp. 3271–3278.

[32] R. W. Erickson and D. Maksimovic, *Fundamentals of Power Electronics*, 2nd ed. Berlin, Germany: Springer, 2007.

[33] E. Waffenschmidt and T. Staring, "Limitation of inductive power transfer for consumer applications," in *Proc. IEEE Eur. Conf. Power Electron. Appl.*, 2009, pp. 1–10.

[34] L. Gu, "Design considerations for radio frequency power converters," Ph.D. dissertation, Dept. Elect. Eng., Stanford Univ., Stanford, CA, USA, 2019.

[35] N. Sokal and A. Sokal, "Class E—A new class of high-efficiency tuned single-ended switching power amplifiers," *IEEE J. Solid-State Circuits*, vol. 10, no. 3, pp. 168–176, Jun. 1975.

[36] Z. Kaczmarczyk, "High-efficiency class E, EF_2, and E/F_3 inverters," *IEEE Trans. Ind. Electron.*, vol. 53, no. 5, pp. 1584–1593, Oct. 2006.